Turk J Phys
28 (2004) , 289 – 299.


# Analysis of RGU Photometry in Selected Area 51

**S. BİLİR[1]*, S. KARAALİ[1] and R. BUSER[2]**
[1] *İstanbul University Science Faculty, Department of Astronomy and Space Sciences, 34119 İstanbul-TURKEY*
*e-mail: sbilir@istanbul.edu.tr*
[2] *Astronomisches Institut der Universität Basel, Venusstrasse 7 4102 Binningen-SWITZERLAND*

Received 03.05.2004

**Abstract**

A low-latitude anticenter field ($l = 189°$, $b = +21°$) is investigated by using the full calibration tools of RGU photometry. The observed RGU data are reduced to the standard system and the separation of dwarfs and evolved stars is carried out by an empirical method. Stars are categorized into three metallicity classes, i.e. $-0.25 < [M/H] \leq +0.50$, $-1.00 < [M/H] \leq -0.25$, and $[M/H] \leq -1.00$ dex, and their absolute magnitudes are determined by the corresponding color-magnitude diagrams. The unusually large scattering in the two-color diagrams is reduced by excluding 153 extra-galactic objects, identifying them compared with the charts of Basel Astronomical Institute and University of Minnesota, and by the criterion and algorithm of Gaidos et al. [1]. The local logarithmic space density for giants, $D^*(0) = 6.75$, lies within the local densities of Gliese and Gliese & Jahreiss. The local luminosity function in our work for the absolute magnitude interval $3 < M(G) \leq 7$ agrees with Hipparcos' luminosity function better than Gliese's luminosity function, whereas it is larger than these luminosity functions for the interval $7 < M(G) \leq 8$. This discrepancy may be due to many reasons, i.e. cumulative catalog errors, binarity etc.

**Key Words:** Galaxy: structure – Stars: luminosity function – Photometry: RGU

## 1. Introduction

Buser's [2] photographic RGU system is a systematic work based on synthetic photometry (Buser [3]). Galactic fields can be investigated through the method given by Buser & Fenkart [4], thus main-sequence stars can be separated into three categories: thin disk, thick disk, and halo, with available absolute magnitudes and metallicities. In addition, the standardized catalogs for 14 fields, properly selected from the Basel Halo Program, are recently used for constructing a new Galactic model (Buser et al. [5, 6]). The lack of calibration of evolved stars (sub-giants and giants) in the work of Buser & Fenkart [4] is compensated by Buser et al. [7], but without giving a method for their separation.

While standard star count analysis provide a description of the present structure of the Galaxy, additional data such as kinematics and chemical abundance are required for understanding the formation and evolution of our Milky Way Galaxy. Although Buser's RGU photometry provides the metallicity distribution of field

*Corresponding author

stars, it does not have an index suitable to the surface gravity, hence the separation of dwarfs (main-sequence stars) and evolved stars requires an indirect method (Karaali [8], Ak et al. [9], Karataş et al. [10], Karaali et al. [11], and Karataş et al. [12]).

Excess of the luminosity function for absolutely faint magnitudes, i.e. $M(G) > 6$ mag, had been used as a clue for such a separation in many works (Fenkart [13–16]) and apparently bright stars (roughly $G < 15-16$ mag) with $M(G) > 6$ mag on the main-sequence had been adopted as evolved stars with correspondingly brighter absolute magnitudes. A few iterations are sufficient to obtain a luminosity function agreeable with the luminosity functions of the Gliese [17] and Hipparcos data [18].

Comparison of Basel and Minnesota charts revealed that there is a considerable number of extra-galactic objects in the star fields which cause an excess in the density and luminosity functions Bilir et al. [19]. Hence, we applied the same procedure to eliminate such objects in our field. It turned out that 153 sources are extra-galactic objects, e.g. galaxies, occupying different regions in the two-color diagrams. However, the scattering in the two-color diagram could not be reduced by the elimination of these objects. Hence, we adopted the distance from the stellar locus criterion and the algorithm of Gaidos et al. [1] (see also Newberg & Yanny [20]) for the reduction of the scattering. As stated by these authors stars concentrate in a band, whereas extra-galactic objects lie out of it. The cited authors used this criterion to obtain a homogenious stellar sample. In our case, although we do not exclude the possibility of scattered objects to be extra-galactic objects, they may well be binary stars, stars with large magnitude errors etc., whose positions result erroneous parameters, such as absolute magnitude. Hence, we excluded them from statistics (see Section 3 for detail). Thus, recovery of the local luminosity function as given by Gliese [17] and/or Hipparcos [18] could be possible.

Section 2 is devoted to observations, reductions, and standardizations. Two-color diagrams are given in Section 3, where the identification of extra-galactic objects, by comparison of the charts of Basel Astronomical Institute and Minnesota University, as well as the treatment of statistical scatter of stellar colors by means of criterion and algorithm of Gaidos et al. [1], is carried out. The separation of dwarfs and evolved stars and their absolute magnitude determination, and density and luminosity functions are given in Sections 4 and 5, respectively. Finally, summary and conclusion is presented in Section 6. We derived the nature and distribution of stars in this field by applying the full calibration tools of RGU photometry, and we hope that this work will be of use to others in their work through a concrete achievement.

## 2. Observations, Reductions, and Standardization

The coordinates of the field with size 0.45 square degrees are $\alpha = 07^h\ 28^m$, $\delta = +29^\circ\ 55'$; $l = 189^\circ$, $b = +21^\circ$ (1950). 1737 stars were measured by one of us (S.K.) in 1995 at the Basel Astronomical Institute down to a apparent magnitude $G = 19$ on each of five plates for each band, i.e. $R$, $G$ and $U$. 50 stars photoelectrically measured by Purgathofer [21] with 19.00, 18.65, and 17.65 as the faintest $U-$, $B-$, and $V-$ magnitudes have been used as standards and their UBV data were transformed to the RGU-system by means of Buser's [22] formulae. The corresponding faintest $R$-, $G$- and $U$- magnitudes are 16.98, 18.25, and 20.09, respectively. The mean catalog errors are given in Table 1. The $(U-B, B-V)$ two-color diagram for standards reveals a color-excess of $E(B-V) = 0^m.03$ which corresponds to $E(G-R) = 0^m.04$ in RGU (Buser [2]). This value is close to those of Schlegel et al. [23], $E(B-V) = 0^m.064$, and Burnstein & Heiles [24], $E(B-V) = 0^m.06$, who used different methods for their derivations, however. The first one is a model value, whereas the second one is derived from the $E(B-V)$ reddening contours with scale 0.03 mag.

$\Delta G$ versus $(G-R)_{obs}$ in Figure 1a give no indication for a color-equation for $G$, whereas there is a linear relation between $\Delta R$ versus $(G-R)_{obs}$, i.e. $\Delta R = -0.11(G-R)_{obs} + 0.14$ (Figure 1b), and a step function between $\Delta U$ versus $(U-G)_{obs}$ (Figure 1c) as follows, where $\Delta m$ (m = $G$, $R$, and $U$) is the difference between the standard ($m_s$) and observed ($m_{obs}$) apparent magnitudes, and $(G-R)_{obs}$ and $(U-G)_{obs}$ are the observed color-indices: $\Delta U = +0.08$, 0.00, -0.01, and +0.05 for $(U-G)_{obs} \leq 1.00$, $1.00 < (U-G)_{obs} \leq 1.65$,

$1.65 < (U-G)_{obs} \leq 2.20$, and $2.20 < (U-G)_{obs}$, respectively.

**Table 1.** Mean catalog errors.

| $G$ interval | $(G)_{err}$ | $(G-R)_{err}$ | $(U-G)_{err}$ |
|---|---|---|---|
| <12 | ± 0.02 | ± 0.02 | ± 0.03 |
| (12-14] | 0.02 | 0.02 | 0.03 |
| (14-16] | 0.02 | 0.03 | 0.02 |
| >16 | 0.03 | 0.04 | 0.03 |

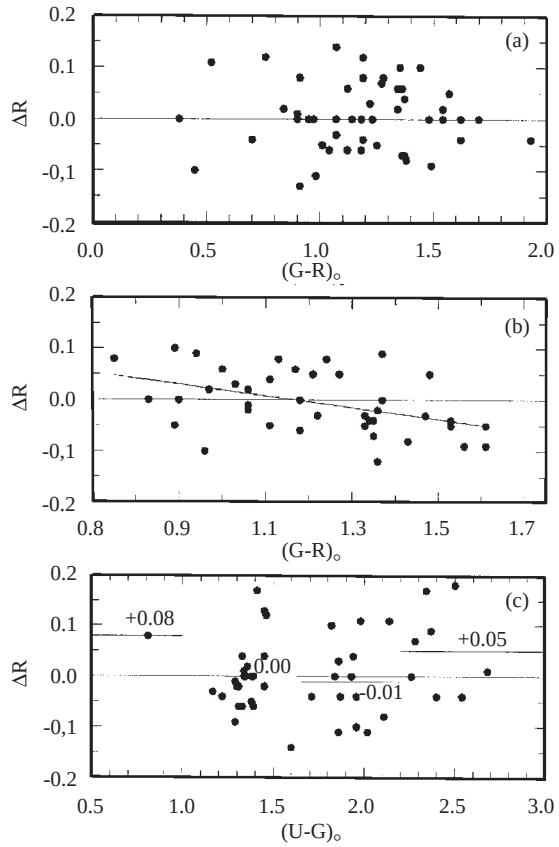


**Figure 1.** Standardization of the data. (a) shows there is no indication for any color equation for G, whereas there is a linear relation between $\Delta R$ versus $(G-R)_{obs}$ in (b), and a step function between $\Delta U$ versus $(U-G)_{obs}$ in (c).

All the RGU data are reduced to the standard system by applying the corrections mentioned above. Thus, all magnitudes and colors which will be used, henceforth are dereddened and standard magnitudes.

## 3. Two-Color Diagrams

The two-color diagrams are drawn within the limiting apparent magnitude of $G = 18$ for consecutive $G$-apparent magnitude intervals, where four of them, i.e. (14.0–15.0], (15.5–16.0], (16.5–17.0], and (17.5–18.0] are given in Figure 2, respectively, as examples. As cited in Section 1, there is an unusually large scatter in these diagrams for low latitude field ($b = +21°$), especially in the location of metal-poor stars in apparently faint magnitude intervals. The comparison of the charts of the Basel Astronomical Institute and Minnesota University reveals that 153 of 1737 objects are extra-galactic objects. However, omitting these

objects does not reduce the scattering considerably, because they lie within the region occupied by stars, i.e. $-3.0 < [M/H] < +0.5$ dex. The extra-galactic objects in the two-color diagrams given in Figure 2 are marked with a different symbol (△).

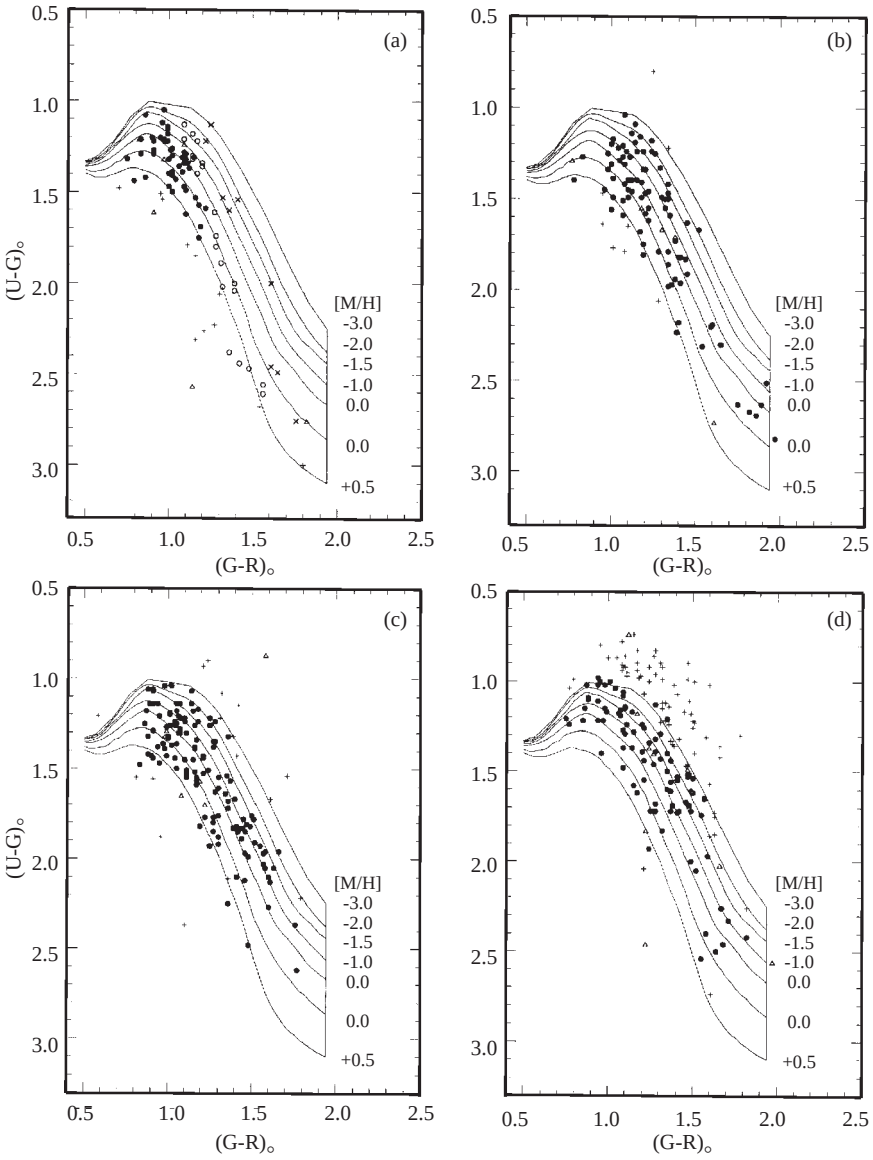


**Figure 2.** Four two-color diagrams as examples, for (14.0–15.0] (a), (15.5–16.0] (b), (16.5–17.0] (c), and (17.5–18.0] (d). There is an unusually large scatter, especially in the faintest apparent magnitude interval, in the location of metal-poor stars. Symbols: (•) dwarfs, (o) sub-giants, (x) late-type giants, (△) extra-galactic objects, and (+) this not included in the statistics.

The luminosity function for all stars (without extra-galactic objects) within the limiting apparent magnitude, $G = 18$, (Figure 5b) resulting from the comparison of density functions with model gradients (see Section 5) Buser et al. [5, 6] (henceforth, BRK) deviates systematically from that of Gliese [17], i.e. there is an excess of absolutely faint stars, $M(G) > 6$, and deficiency of absolutely bright stars, $M(G) < 5$, indicating that the scattering affected the absolutely bright stars to shift to the region of faint ones. It is worth noting that this is what we had experienced in our other works (cf. Fenkart & Karaali [25]).

We applied the *distances from the stellar locus* criterion and the algorithm of Gaidos et al. [1] (see also Newberg & Yanny [20]) with a slight modification and purpose, however, to reduce the number of scattered stars. These authors formed a locus of all pointlike sources in the multi-color space and they fitted a set of locus points along the center of the locus of these sources. The stellar candidates selected were those that were closer to their associated locus point than the metric distance $d$ (a parameter to be determined) in magnitudes for all colors, whereas the quasi-stellar object candidates were the ones at distances larger than $d$. In our case, we applied this criterion and algorithm to the color-plane, i.e. $(U-G, G-R)$ two-color diagram, and adopted the metric distance as $d = 1.3s$, where $s$ is the standard deviation for each color, for each sub-sample of stars (separated by dashed lines in Figure 3b). Thus, stars for each sub-sample, within at least $1s$ were included in the statistics (see Table 2 for their percentages). Figure 3a gives all dwarfs in the field SA 51, and Figure 3b those selected by the criterion and algorithm of Gaidos et al. [1]) for statistical purpose.

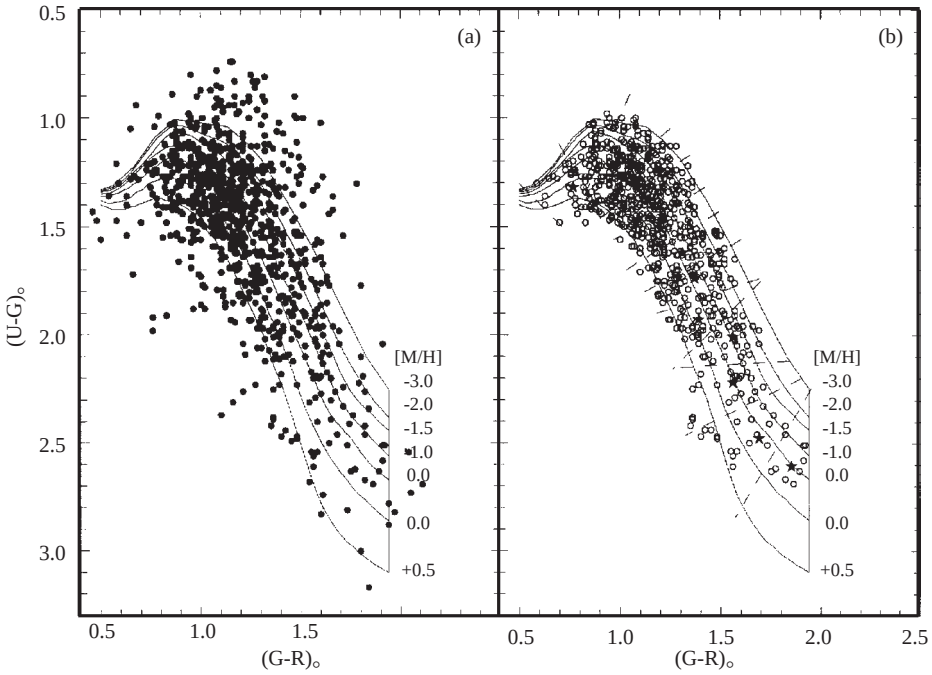


**Figure 3.** Two-color diagram for dwarfs brighter than the apparently limiting magnitude, $G = 18$ mag. (a) for all stars, (b) for stars included into statistics, i.e. within the distance $d = 1.3s$, for $U-G$, and $G-R$ colors, from the corresponding locus point associated. The symbol ($\star$) denotes the locus point and the dashed lines separate dwarfs into sub-samples with centroid ($\star$). $s$ is the standard deviation for each color, for the corresponding sub-sample.

# 4. Dwarf-Giant Separation and Absolute Magnitude Determination

Dwarfs and late-type giants were separated by the gap criterion (Becker [26]), whereas no effort was carried out for the separation of sub-giants. Late-type giants were recognized by their location separated from dwarfs by a gap and with larger $U-G$ color-indices relative to the main-sequence with $[M/H] \sim 0.0$ dex, in the $(U-G, G-R)$ two-color diagrams for low-latitude fields (cf. Becker & Fang [27]; Hersperger [28]). However, Becker [29] showed that there exists another type of late-type giant, lying at the metal-poor region of the two-color diagram, and a bit bluer than the ones mentioned above; thus a bit disregarding the gap which separates dwarfs and metal-rich late-type giants. During the epoch of comparison the density functions with the galactic models, the local logarithmic space density for late-type giants, i.e. $\odot = 6.64$

(Gliese [17]), was the favorite clue for their separation (Del Rio & Fenkart [30]; Fenkart [13–16]; Fenkart & Karaali [25]).

**Table 2.** The $U-G$, $G-R$ color-indices of the locus points (W), number of stars, for each sub-sample associated with them ($N^{'}$) and within the distance $d = 1.3s$ from the corresponding locus point (N), and the percentage of stars included into statistics ($s$ is the standard deviation for each color for the sub-sample considered).

| W | $U-G$ | $G-R$ | $N^{'}$ | N | % |
|---|---|---|---|---|---|
| 1 | 1.32 | 0.77 | 30 | 20 | 67 |
| 2 | 1.14 | 0.87 | 50 | 41 | 82 |
| 3 | 1.17 | 1.00 | 107 | 76 | 71 |
| 4 | 1.28 | 1.07 | 146 | 133 | 91 |
| 5 | 1.38 | 1.14 | 144 | 108 | 75 |
| 6 | 1.51 | 1.20 | 100 | 81 | 81 |
| 7 | 1.62 | 1.31 | 67 | 53 | 79 |
| 8 | 1.74 | 1.37 | 81 | 62 | 77 |
| 9 | 1.93 | 1.39 | 53 | 41 | 77 |
| 10 | 2.01 | 1.56 | 38 | 29 | 76 |
| 11 | 2.22 | 1.56 | 25 | 18 | 72 |
| 12 | 2.48 | 1.69 | 22 | 19 | 86 |
| 13 | 2.61 | 1.85 | 10 | 8 | 80 |

Systematic deviation of the luminosity functions from the one of Gliese [17] revealed that the absolutely faint segment of the luminosity function was contaminated by evolved stars (sub-giants and giants), resulting in an excess for $M(G) > 6$ mag and a deficiency for $M(G) < 5$ mag in the luminosity function. This disagreement was used as a clue for the separation of dwarfs and evolved stars in recent years (Karaali [8], Ak et al. [9], Karataş et al. [10], Karaali et al. [11], and Karataş et al. [12]). The fundamental assumption for this empirical method is that apparently bright and absolutely faint stars on the main-sequence are evolved. In this work, a few iterations provided a luminosity function in best agreement with the local luminosity function as given by Gliese [17] and/or Hipparcos [18] by assuming that for apparent magnitudes brighter than $G = 15.5$ mag, stars which according to their positions in the two-color diagram could be identified as dwarfs with assigned absolute magnitudes fainter than $M(G) = 6$ mag, are however most likely evolved stars with correspondingly brighter absolute magnitudes.

Following Buser & Fenkart [4], we separated dwarfs into three metallicity classes: $-0.25 < [M/H] \leq +0.50$ dex (Thin Disk), $-1.00 < [M/H] \leq -0.25$ dex (Thick Disk), and $[M/H] \leq -1.00$ dex (Halo), and we used their corresponding color-magnitude diagram, derived from extent sources via synthetic photometry, for absolute magnitude determination. Contrary to the works investigated in Steinlin's [31] system, individual absolute magnitudes are adopted for late-type giants (and sub-giants) by separating them into different metallicity-classes and using the multi-metallicity color-magnitude diagram of Buser et al. [7], derived in the same way as dwarfs.

## 5. Density and Luminosity Functions

The logarithmic space densities $D^* = \log D(r) + 10$ are evaluated for five absolute magnitude intervals, i.e. (3–4], (4–5], (5–6], (6–7] and (7–8], where the absolute magnitudes are complete, and for late-type giants (see Tables 3 and 4). However, the number of stars for the absolute magnitude intervals (2–3], (8–9], and (9–10] for each distance interval is also given in Table 3. Here $D = N/\Delta V_{1,2}$, $N$ being the number of

stars, found in the partial volume $\Delta V_{1,2}$ which is determined by its limiting distances $r_1$ and $r_2$, and by the apparent field size in square degrees $A$, i.e. $\Delta V_{1,2} = (\pi/180)^2(A/3)(r_2^3 - r_1^3)$.

**Table 3.** The logarithmic space densities $D^* = \log D + 10$ for five absolute magnitude intervals, i.e. (3–4], (4–5], (5–6], (6–7], and (7–8] for dwarfs and sub-giants, where the absolute magnitudes are complete. Thick horizontal lines: limiting distance of completeness (for definition of the symbols see text; distances in kpc; volumes in $pc^3$).

| | | $M(G) \rightarrow$ | (2–3] | | (3–4] | | (4–5] | | (5–6] | | (6–7] | | (7–8] | | (8–9] | | (9–10] | |
|---|---|---|---|---|---|---|---|---|---|---|---|---|---|---|---|---|---|---|
| $r_1$-$r_2$ | $\Delta V_{1,2}$ | $\bar{r}$ | N | D* | N | D* | N | D* | N | D* | N | D* | N | D* | N | D* | N | D* |
| 0.00-0.40 | 2.88 (3) | 0.32 | | | 3 | 7.02 | | | 7 | 7.39 | | | | | 19 | – | 4 | – |
| 0.00-0.63 | 1.15 (4) | 0.50 | | | | | 9 | 6.89 | | | | | 35 | 7.48 | | | | |
| 0.00-1.00 | 4.57 (4) | 0.79 | | | | | | | | | 44 | 6.98 | | | | | | |
| 0.40-0.63 | 8.60 (3) | 0.54 | | | 2 | 6.37 | | | 11 | 7.11 | | | | | 28 | – | 3 | – |
| 0.63-1.00 | 3.42 (4) | 0.86 | | | 7 | 6.31 | 13 | 6.58 | 39 | 7.06 | | | 46 | 7.13 | 15 | – | | |
| 1.00-1.59 | 1.36 (5) | 1.36 | | | 10 | 5.87 | 27 | 6.30 | 45 | 6.52 | 80 | 6.77 | 24 | 6.25 | | | | |
| 1.59-2.51 | 5.42 (5) | 2.15 | 4 | – | 20 | 5.57 | 23 | 5.63 | 42 | 5.89 | 28 | 5.71 | | | | | | |
| 2.51-3.98 | 2.16 (6) | 3.40 | 4 | – | 19 | 4.94 | 20 | 4.97 | 14 | 4.81 | | | | | | | | |
| 3.98-6.31 | 8.59 (6) | 5.40 | 1 | – | 9 | 4.02 | 7 | 3.91 | | | | | | | | | | |
| | | Total | 9 | | 70 | | 99 | | 158 | | 152 | | 105 | | 62 | | 7 | |

The density functions are most appropriately given in the form of histograms whose sections with ordinates $D^*(r_1, r_2)$ cover the distance-intervals $(r_1, r_2)$, and heavy dots on the histogram sections $D^*(r_1, r_2)$ designate the centroid-distance $\bar{r} = [(r_1^3 + r_2^3)/2]^{1/3}$ of the corresponding partial volume $\Delta V_{1,2}$ (Del Rio & Fenkart [30]; Fenkart & Karaali [25]; and Fenkart [13–16]).

The density functions are compared with the galactic model of BRK, in the form $\Delta \log D(r) = \log D(r, l, b) - \log D(0, l, b)$ versus $r$, where $\Delta \log D(r)$ is the difference between the logarithmic densities at distance $r$ and at the Sun. Thus, $\Delta \log D(r) = 0$ points out the logarithmic space density for $r = 0$ which is available for local luminosity function determination. The comparison is carried out as explained in some works of Basel fields (Del Rio & Fenkart [30]; Fenkart & Karaali [25], i.e. by shifting the model curve perpendicular to the distance axis until the best fit to the histogram results at the centroid distances (Figure 4).

Figure 4 show that there is good agreement between the model gradients and the observed density histograms. The same agreement holds when local densities are considered, except for the absolute magnitude interval $7 < M(G) \leq 8$. This can be confirmed by comparison of the local luminosity function with the luminosity function of Gliese [17] and Hipparcos [18]. In Figure 5, there are two luminosity functions resulting from comparisons of observed density histograms for dwarfs and sub-giants with the best-fitting model gradients BRK. For (a) we used the data in Table 3 and Figure 4a–e, where unusual scattering in the two-color diagrams is reduced by the criterion and algorithm of Gaidos et al. [1]; for (b), all dwarfs and sub-giants within the limiting apparent magnitude, $G = 18$, are used. The agreement is much better for (a). The luminosity (a) for the interval $5 < M(G) \leq 6$, is almost equal to those of Gliese and Hipparcos and close to them for the interval $6 < M(G) \leq 7$, but it is a bit deficient relative to the luminosity function of Hipparcos for the segment $3 < M(G) \leq 5$ (the luminosity function of Hipparcos is also deficient relative to the luminosity function of Gliese for the same absolute magnitude interval). However, there is a considerable excess for the luminosity function (a) relative to both luminosity functions of Gliese and Hipparcos for the interval $7 < M(G) \leq 8$, i.e. 0.30 in units of logarithmic space density, which is much larger than the standard deviation for this absolute magnitude interval (Table 5). It is worth noting that the differences between the luminosity function (a) and that of Hipparcos for other absolute magnitude intervals, are all less than the corresponding standard deviations given in Table 5. Although the luminosity function (b) is close to the luminosity function (a) for the absolute magnitude intervals (3–4], (4–5], and (5–6], it deviates from (a) for two absolutely faint magnitude intervals, i.e. (6–7], and (7–8], considerably.

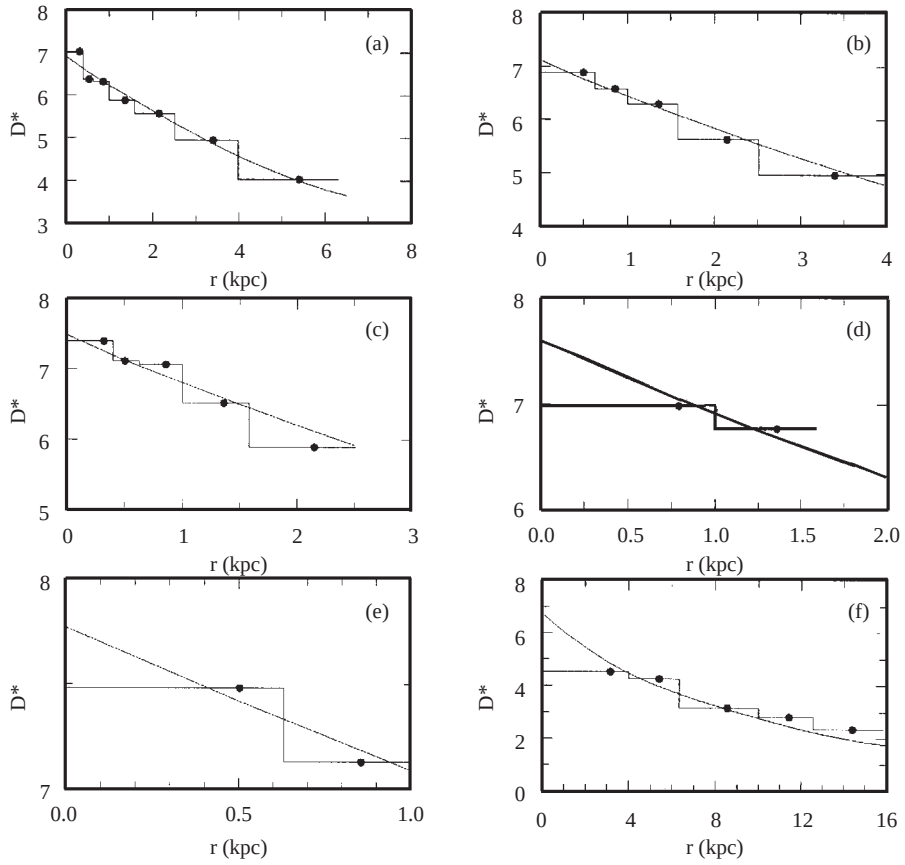


**Figure 4.** Logarithmic space-density histograms for dwarfs and sub-giants of different absolute-magnitude intervals: (3–4] (a), (4–5] (b), (5–6] (c), (6–7] (d), (7–8] (e), and for late-type giants (f). Bullets (•) denotes the centroid distance within the limiting distance of completeness, for comparison with model gradients BRK.

**Table 4.** The logarithmic space density $D^* = \log D + 10$ for late-type giants (see text for definition of the symbols; distances in kpc; volumes in pc$^3$)

| $r_1$-$r_2$ | $\Delta V_{1,2}$ | $\bar{r}$ | N | $D^*$ |
|---|---|---|---|---|
| 0-3.98 | 2.88 (6) | 3.16 | 10 | 4.54 |
| 3.98-6.31 | 8.60 (6) | 5.40 | 16 | 4.27 |
| 6.31-10.00 | 3.42 (7) | 8.55 | 5 | 3.16 |
| 10.00-19.95 | 3.17 (8) | 16.48 | 6 | −− |

**Table 5.** Local luminosity function resulting from comparison of observed histograms with best-fitting model gradients BRK, and confronted to Gliese [17] and Hipparcos [18] local luminosity functions. $s$ is the standard deviation in units of logarithmic space density.

| $M(G) \rightarrow$ | (3-4] | (4-5] | (5-6] | (6-7] | (7-8] |
|---|---|---|---|---|---|
| BRK | 6.91 | 7.12 | 7.48 | 7.55 | 7.77 |
| $s$ (±) | 0.17 | 0.12 | 0.16 | 0.17 | 0.08 |
| Gliese [17] | 7.18 | 7.41 | 7.52 | 7.48 | 7.42 |
| Hipparcos [18] | 7.04 | 7.20 | 7.47 | 7.47 | 7.47 |

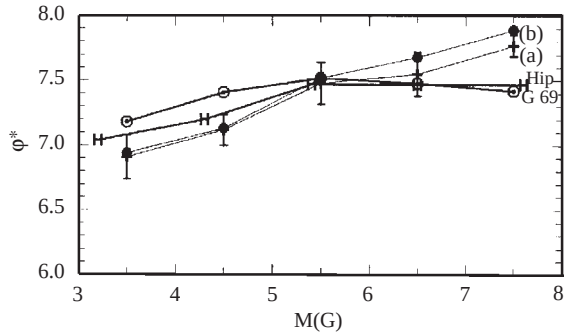


**Figure 5.** Two luminosity functions resulting from comparison of observed histograms with best-fitting model gradients BRK, and confronted to Gliese [17] (⊙), and Hipparcos [18] (H); (a) for dwarfs and sub-giants for which unusual scattering in the two-color diagrams is reduced by the criterion and algorithm of Gaidos et al. [1] (taken from Table 3), and (b) for all dwarfs and sub-giants in the two-color diagrams within the limiting apparent magnitude, $G = 18$ (the density functions for (b) have not been given to conserve space).

The comparison of the density function for giants with the model gradients BRK is carried out up to $r = 10$ kpc (Figure 4f). Six stars within the large distance interval $10.00 < r \leq 19.95$ kpc are not included in the statistics. The local density resulting from this comparison, $D^*(0) = 6.75$, lies between the local densities of Gliese [17] and Gliese & Jahreiss [32], i.e. $\odot = 6.64$ and $\odot = 6.92$, respectively.

# 6. Summary and Conclusion

We used the full calibration tools of RGU photometry to investigate the low-latitude ($b = +21°$) and anticenter ($l = 189°$) field SA 51. The observed RGU data are reduced to the standard system and the separation of dwarfs and evolved stars is carried out by an empirical method, based on the assumption that apparently bright stars are evolved (Karaali [8], Ak et al. [9], Karataş et al. [10], Karaali et al. [11], and Karataş et al. [12]), i.e. for apparent magnitudes brighter than $G = 15.5$ mag stars which, according to their positions, are identified as dwarfs with assigned absolute magnitude fainter than $M(G) = 6$ mag, and are however most likely evolved stars with corresponding brighter absolute magnitudes. This assumption provided a luminosity function agreeable with the local luminosity function as given by Gliese [17] and Hipparcos [18]. Dwarfs are separated into three metallicity classes, i.e. $-0.25 < [M/H] \leq +0.50$ dex (Thin Disk), $-1.00 < [M/H] \leq -0.25$ dex (Thick Disk), and $[M/H] \leq -1.00$ dex (Halo), and their absolute magnitudes are determined by the corresponding color-magnitude diagrams of Buser & Fenkart [4], derived from extent sources via synthetic photometry. The metallicities and absolute magnitudes for evolved stars are evaluated by the recent diagrams of Buser et al. [7].

Although 153 extra-galactic objects were excluded from the complete sample, compared with the charts of Basel Astronomical Institute and Minnesota University (Bilir et al. [19]), the scattering in the two-color diagrams could not be reduced. We applied the criterion and algorithm of Gaidos et al. [1] to the color-plane, i.e. $(U-G, G-R)$ two-color diagram, to reject dwarfs at distances in magnitude larger than $d = 1.3s$ from the center of the locus of all dwarfs in the direction to $U-G$ and $G-R$ axes, where $s$ is the standard deviation of dwarfs associated with the locus point in each sub-sample (separated by dashed lines in Figure 3b). This limitation reduced dwarfs by 79%, which is larger than the percentage in $1s$ for a gaussian distribution.

The density histograms for dwarfs and sub-giants with absolute magnitudes (3–4], (4–5], (5–6], (6–7], and (7–8] agree with the model gradients BRK. The same agreement holds when local densities are considered, except for the absolute magnitude interval $7 < M(G) \leq 8$, where the luminosity has an excess of 0.30 in units of logarithmic density relative to the luminosity of Hipparcos. The number of dwarfs in this interval

can not be reduced, otherwise they turn out to be giants with density function contradicting with the model gradients BRK and local density different than the ones of Gliese [17] and Gliese & Jahreiss [32].

One of the reasons for the deviation of the luminosity function for the interval $7 < M(G) \leq 8$ from Gliese's [17] or Hipparcos' [18] may be binarity, or other properties such as cumulative catalog errors etc. We refer to Buser & Kaeser [33], who were the first to consider the effects of unresolved stars in the far-field surveys and luminosity functions. It may require the comparison of the luminosity functions with an appropriately redetermined local one via the data of Gliese [17] or Hipparcos [18].

The luminosity function in our work is much better than the one in Karataş et al. [10]. All the tools used for the investigation of two fields are the same, except the distance criterion and algorithm of Gaidos et al. [1] which is used only in our work. This new approach can be useful for understanding the nature of stars in the fields treated.

Acknowledgments: We would like to thank Schweizerischer Nationalfonds zur Förderung der Wissenschaflichen Forschung, and the Scientific and Technical Research Council of Turkey for financial support (TBAG-AY/74), and the University of Minnesota for providing us with its APS on-line catalogs for the investigated field.

# References

[1] E. J. Gaidos, E. A. Magnier and P. L. Schechter, *PASP,* **105,** (1993), 1294.

[2] R. Buser, *A&A,* **62,** (1978), 425.

[3] R. Buser, PhD. Thesis, Astronomisches Institut der Universität Basel, Switzerland, 1975.

[4] R. Buser and R. P. Fenkart, *A&A,* **239,** (1990), 243.

[5] R. Buser, J. Rong and S. Karaali, *A&A,* **331,** (1998), 934 (BRK).

[6] R. Buser, J. Rong and S. Karaali, *A&A,* **348,** (1999), 98.

[7] R. Buser, Y. Karataş, Th. Lejeune, J. X. Rong, P. Westera and S. G. Ak, *A&A,* **357,** (2000), 988.

[8] S. Karaali, VIII. Nat. Astron. Symp. Eds. Z. Aslan and O. Gölbaşı, Ankara-Turkey, (1992), p.202.

[9] S. G. Ak, S. Karaali and R. Buser, *A&AS,* **131,** (1998), 345.

[10] Y. Karataş, S. Karaali and R. Buser, *A&A,* **373,** (2001), 895.

[11] S. Karaali, S. Bilir and R. Buser, *PASA,* **21,** (2004), 275.

[12] Y. Karataş, S. Bilir, S. Karaali and S. G. Ak, *AN*, (2004) (accepted).

[13] R. P. Fenkart, *A&AS,* **78,** (1989), 217.

[14] R. P. Fenkart, *A&AS,* **79,** (1989), 51.

[15] R. P. Fenkart, *A&AS,* **80,** (1989), 89.

[16] R. P. Fenkart, *A&AS,* **81,** (1989), 187.

[17] W. Gliese, Veröff. Astron. Rechen Inst. Heidelberg, (1969), No:22.

[18] H. Jahreiss and R. Wielen, in: HIPPARCOS'97. Presentation of the HIPPARCOS and TYCHO catalogues and first astrophysical results of the Hippaccos space astrometry mission, B. Battrick, M. A. C. Perryman and P. L. Bernacca, (eds.), ESA SP-402, Noordwÿk, (1997), p.675 (JW).

[19] S. Bilir, Y. Karataş and S. G. Ak, *TJPh,* **27,** (2003), 235.

[20] H. J. Newberg and B. Yanny, *ApJS,* **113,** (1997), 89.

[21] A. Th. Purgathofer, *Bulletin/Lowell Observatory,* **7,** (1969), No: 147, p.98.

[22] R. Buser, in, Fresneau A., Hamm M. (eds.) Impacts des surveys du visible sur notre connaissance de la Galaxie. Comptes rendus sur les Journees de Strasbourg, 9eme Reunion, Obs. de Strasbourg, (1988), p.15.

[23] D. J. Schlegel, D. P. Finkbeiner and M. Davis, *ApJ,* **500,** (1998) 525.

[24] D. Burnstein and C. Heiles, *AJ,* **87,** (1982), 1165.

[25] R. P. Fenkart and S. Karaali, *A&AS,* **69,** (1987), 33.

[26] W. Becker, *ZA,* **54,** (1962), 155.

[27] W. Becker and Ch. Fang, *A&A,* **22,** (1973), 187.

[28] Th. Hersperger, *A&A,* **22,** (1973), 195.

[29] W. Becker, *A&AS,* **38,** (1979), 341.

[30] G. Del Rio and R. P. Fenkart, *A&AS,* **68,** (1987), 397.

[31] U. W. Steinlin, *ZA,* **69,** (1968), 276.

[32] W. Gliese and H. Jahreiss, Third Catalogue of Nearby Stars (Preliminary Version), Astron. Rechen Inst. Heidelberg, (1992).

[33] R. Buser and U. Kaeser, *A&A,* **145,** (1985), 1.